Morphology and High-temperature Stability of an Amorphous Alumina Coating Deposited by Metal Organic Chemical Vapor Deposition on Various Substrates

BY

Justin Daniel Meyer

A THESIS

Submitted to the Faculty of Stevens Institute of Technology
in partial fulfillment of the requirements for the degree of

MASTER OF ENGINEERING

_____
Justin Daniel Meyer, Candidate

ADVISORY COMMITTEE

_____
Prof. Woo Young Lee   Date

_____
Prof. Henry Du   Date

STEVENS INSTITUTE OF TECHNOLOGY
Castle Point on Hudson, Hoboken, NJ 07030
2000

Morphology and High-temperature Stability of an Amorphous Alumina Coating Deposited by Metal Organic Chemical Vapor Deposition on Various Substrates

ABSTRACT

Aluminum acetylacetonate and water vapor were used to deposit an amorphous alumina (Al_2O_3) coating on a single crystal silicon (Si) wafer and a nickel super alloy, a porous CeO_2-stabilized ZrO_2 (CSZ) coating produced by air plasma spray (APS), and polished silicon carbide (SiC). The Al_2O_3 coating prepared at ~500°C was uniform and non-porous. The crystallization and adhesion characteristics of the Al_2O_3 coating were examined by thermally annealing the Al_2O_3-coated substrates in air. The amorphous coating crystallized to metastable Al_2O_3 phases within 20 hours at temperatures as low as 700°C. The Al_2O_3 coating thicker than ~1μm on Si spalled upon annealing whereas the coating on CSZ did not spall but microcracked extensively due to the significant volume shrinkage associated with crystallization. Coatings on the René N5 nickel super alloy and silicon carbide exhibited unique morphological characteristics but remained adherent after annealing. In contrast, the coating with a thickness less than 200nm exhibited superior morphological stability, and may be adapted to a multi-annealing-step process for sealing highly porous CSZ microstructures.

Justin Daniel Meyer, Master of Engineering

Department of Chemical, Biochemical, and Materials Engineering

Advisor: Professor W.Y. Lee

May, 2000

ACKNOWLEDGMENTS

I would like to thank my thesis advisor, Professor Woo Lee, for his continued support and advice throughout the duration of this thesis work. Prof. Lee's unwavering guidance and understanding have been integral to the success of my work.

Professor Henry Du provided valuable advice and participated graciously on my thesis committee. Many thanks also go to Prof. Traugott Fischer for his advice and encouragement throughout the past two years.

Also, I am also indebted to my colleagues, Mr. Gi Youl Kim, Mr. Jinil Lee, and Mr. Limin He for their assistance and many fruitful discussions. And the assistance of members of the Microscopy Group, Mr. Alex Chou and Mr. Pipat Prayoonthong, is greatly appreciated.

Further, I would also like to thank Miss Patricia Downes and Mr. Yosif Korogodsky for lending a helpful hand at every request.

During a significant portion of my research time, I was honored to be a recipient of a *Robert C. Stanley Fellowship*. A large portion of this project was funded by Mr. Brad Beardsley at *Caterpillar, Inc*.

TABLE OF CONTENTS

LIST OF FIGURES

LIST OF FIGURES *(Continued)*

LIST OF TABLES

INTRODUCTION

Thermal barrier coatings (TBCs) have been developed to improve the performance of aircraft engines, power generation gas turbines, and diesel engines [1-3] by increasing the energy retained by the combustion volume. For diesel engines, CeO_2-stabilized ZrO_2 (CSZ) is applied by air plasma spray (APS) over a graded NiCrAlY bond coating to insulate and protect cast iron components from high-temperature combustion environments [2]. The APS CSZ coating is made intentionally porous for strain tolerance and for enhanced adhesion at the metal-ceramic interface region. However, recent engine test results have shown that the porous CSZ coating may absorb fuel prior to ignition in the combustion chamber, which may adversely affect overall engine efficiency [2,3].

A pragmatic solution to the fuel entrainment problem is to seal the CSZ surface with a thin coating, just as varnish is used to seal the grain of wood. Such a seal coating must be non-porous, impermeable, conformal, adherent, and stable upon thermal cycling to 800-900°C. Another major constraint is that the seal coating must be prepared at temperatures below 500°C to avoid tempering of cast iron components.

Al_2O_3 is an ideal candidate coating material because: (1) it is one of the most thermochemically stable materials with respect to ZrO_2-based ceramics as well as in high-temperature corrosion environments, and (2) it has a coefficient of thermal expansion (CTE) similar to that of CSZ (~8×10^{-6} versus ~10×10^{-6} K^{-1}, respectively).

However, these attractive properties are reserved mainly for crystalline α-Al_2O_3, which is the only thermodynamically stable polymorph of Al_2O_3. It is generally known that α-Al_2O_3 is a difficult material to prepare by chemical or physical vapor deposition processes unless deposition temperatures above 1000°C are used [4].

Al_2O_3 is also used heavily in the tool industry to prolong the life of WC/Co cutting tool inserts and other materials. The many advantageous characteristics of α-Al_2O_3 make it an ideal coating for numerous applications. However, the coating is useful only if it can be deposited and remain adherent and morphologically stable during both processing and use.

LITERATURE REVIEW

Aluminum oxide (alumina) exists in many different metastable phases between the amorphous and the stable α-Al_2O_3. Those most commonly deposited by the CVD process are amorphous, α-, and γ- Al_2O_3 [4]. There are two prevalent Al precursor systems which have been studied extensively: hydrolysis of aluminum halides (of which $AlCl_3$ is the most widely used and well known) and pyrolysis of metal organic precursors. Each system enjoys its own advantages, mitigated by each of their own processing short-comings.

Hydrolysis of AlCl$_3$

Deposition by hydrolysis of $AlCl_3$ has two main process variations, the first with water introduced directly in vapor form (1), and the second with the introduction of H_2

$$2AlCl_3(g) + 3H_2O(g) \rightarrow Al_2O_3(s) + 6HCl(g) \qquad (1)$$
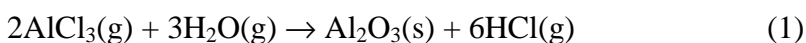
and CO_2 (2). The latter is preferred for its extended deposition range which is due to

$$2AlCl_3(g) + 3H_2(g) + 3CO_2(g) \rightarrow Al_2O_3(s) + 6HCl(g) + 3CO(g) \qquad (2)$$
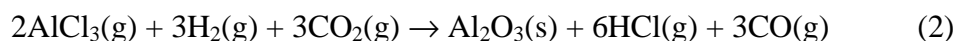
slower deposition kinetics. When using variation (1), there were often multiple phases present in films formed between 750 and 1000°C, these films also tended to be structurally unsound. Variation (2) is far more common, with some work using N_2 as a carrier gas to entrain the $AlCl_3$ vapor. While the processing temperature ranged from 200-1825°C with varying pressure, α-Al_2O_3 has not been reported below ~800°C, and no

metastable phases have been observed below ~500°C [6-13]. Films deposited below 500°C—even as low as room temperature—are often of low quality and contain numerous impurities. The reaction described by equation (2) has also demonstrated a dependence on pressure, as well as a high sensitivity to gas ratios. This is particularly true of the H_2/CO_2 ratio, which affects the H_2O formation rate of the water-gas phase shift reaction (3):

$$H_2 + CO_2 \rightarrow H_2O + CO \tag{3}$$

The use of H_2 and CO_2 mitigates the premature reaction of H_2O with $AlCl_3$, creating an extended reaction "envelope" for deposition. This is particularly advantageous, since this process is notorious for homogeneous nucleation of Al_2O_3 [4]. If desired, the reaction may be accelerated by the inclusion of very small amounts of O_2 [14], but at increased risk of Al_2O_3 nucleating in the gas phase.

Pyrolysis of Metal-Organics
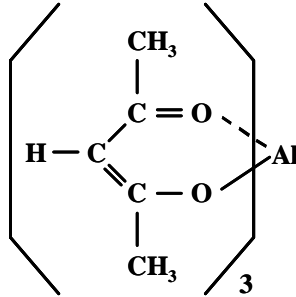
Deposition of crystalline alumina films at lower temperatures has demonstrated marginally higher promise with metal-organic precursor systems. These fall into three main categories: aluminum alkoxides, alkyl compounds, and acetylacetonates [4]. Almost nearly all alkoxides and alkyl compounds tend to deposit porous films, which may also exhibit poor adhesion and a significant number of impurities. Both compound types are sensitive to humidity – alkyls sometimes explosively [15-20]. Few of these disadvantages are observed with aluminum acetylacetonate ($Al(acac)_3$). $Al(acac)_3$ is a white solid which is non-toxic, stable, and relatively moisture insensitive. Further, it

possesses an oxygen-to-aluminum ratio of 2:1 and decomposes readily below 500°C. A more complete list of properties may be observed in Table I.

Despite the wide functional temperature range, films deposited below ~550°C tended to exhibit some carbon contamination. This contamination can be mitigated by the inclusion of extra oxygen in the precursor stream to ensure complete decomposition of the Al(acac)$_3$ upon adsorption to the substrate surface. In addition to increasing the purity of the deposited films, the inclusion of oxygen also increased the deposition rate and film adhesion [21-23]. Complete decomposition of the precursor may be assured by the inclusion of water vapor—resulting in films free from carbon contamination [22].

The use of the metal organic precursor Al(acac)$_3$ offers the widest range of advantages. Its docile and controllable chemical properties make it the most appealing precursor system candidate by far. The only drawback, not unique to this precursor, is the near impossibility of depositing crystalline Al$_2$O$_3$ at the temperatures being used in this work.

Table I. Critical properties* of aluminum acetylacetonate: Al(acac)$_3$.

PROPERTY*	VALUE
Sublimation temperature	150ºC
Melting point	192-193ºC
Toxicity	Low
Reactivity	Low
Moisture sensitivity	Low
Cost	~$100/kg
Molecular weight	324.31 g/mol
Structure	

*As reported in the MSDS provided by Strem Chemicals, Inc.

STATEMENT OF PURPOSE

The main objective of this work was to explore the possibility of using an amorphous Al_2O_3 prepared by metal organic chemical vapor deposition (MOCVD) at ~500°C with emphasis on evaluating the coating's physical integrity upon exposure to high-temperature environments. In particular, the significant volume shrinkage expected from the crystallization of the amorphous Al_2O_3 coating (~ -9%) [5] was a great concern.

Most of the previous collaborations investigating the use of Al_2O_3 in industrial applications were not nearly so constrained by processing temperature as in this study. Once an "ideal" precursor system was found from reviewing previous systems studied, a system was built to meet the processing requirements. The specific tasks during the course of this work included: optimization of system parameters, investigation of the crystallization "path" and the effects of exposure to a high-temperature environment, and determining morphological and mechanical stability with some deference to the role of Al_2O_3 as a seal coating on a porous TBC and other substrates.

PRELIMINARY CONCERNS

Seal Coating Criteria

The finer points of seal coating criteria fall into two categories and encompass both precursor selection and process optimization. The materials criteria mandate that the seal coating be non-porous and impermeable, that it have good adhesion to the CSZ (or other substrate), that it demonstrate high thermal stability, and that it incur no debit to the CSZ strain tolerance and resist erosion and wear. The processing criteria include deposition temperatures below 500°C (this maximum would become our operational ceiling), and maintaining a conformal coating on a complex, porous TBC surface. Previous work by Dr. W.Y. Lee at Oak Ridge National Laboratory compared several candidate coating materials which are listed in the top half of Table II; of these Al_2O_3 exhibiting the most promise.

Experimental Approach

There are several system-specific concerns which need to be taken into account. The most prevalent is potential problems with MOCVD of an Al_2O_3 coating. The deposition of an amorphous coating in itself brings about the expectation of significant volume shrinkage upon crystallization. Further, carbon and hydrogen impurities have been observed in and found to degrade coating integrity, leading to the inclusion of water vapor as a precursor—encouraging complete consumption of the metal organic $Al(acac)_3$ [22].

While the CSZ TBC, nickel alloy, and SiC were being investigated, they showed poor characterization in several key respects. Because of this, Si was included for ease of characterization and processing optimization and analysis, despite the rather large thermal mismatch with Al_2O_3 observed in the bottom half of Table II.

Table II. Coefficients of thermal expansion and moduli of earlier coating candidates and current substrates.

COATING/SUBSTRATE	CTE (*10^{-6}/K)	MODULUS (GPA)
$3Al_2O_3*2SiO_2$ (mullite)	6	145
SiO_2 (fused)	0.5	70
ZrO_2 (monoclinic)	7	138
α-Al_2O_3	8	380
APS-CSZ	~10	~200
Nickel alloy (René N5)	11-13	~210
Si (100)	4	163
SiC (sintered α)	~4.5	~425

EXPERIMENTAL PROCEDURE

Sample Preparation

A large portion of this work was conducted using single crystal silicon (Si) pieces as substrates for ease of characterization during initial coating preparation and evaluation; this is reflected in the reporting of results. The Si samples were from commercial (111)-silicon wafers and boron doped to a resistivity between 8 and 12 ohm-cm. Silicon carbide (SiC) and β-nickel [100] (GE René N5: nominal composition of 6.2 Al, 0.05 C, 7.5 Co, 0.16 Hf, 1.5 Mo, 3.0 Re, 6.5 Ta, 0.02 Ti, 5.0 W, and Ni as the remaining weight percent) samples were also used for coating morphology examination and comparison. Although the Si and SiC samples were pre-polished, the nickel substrates needed to be polished using a five-step polishing regimen with a 0.05μm alumina slurry as the last step. Just prior to deposition, all samples were cleansed using a three-step wash process consisting of methanol (99.8%), iso-propanol (99.5%), and acetone (99.5%).

APS CSZ-coated cast iron flexure bars and free-standing CSZ coupons were also used as substrates to characterize the system's ability to coat a topologically complex substrate. After being subjected to the cleansing regimen described above, these highly porous substrates were allowed to dry in open air for 30 minutes prior to deposition.

MOCVD System

For this work a cold-wall MOCVD system, depicted in Figure 1, was constructed. The reactor was constructed of stainless steel with an internal resistance substrate heater
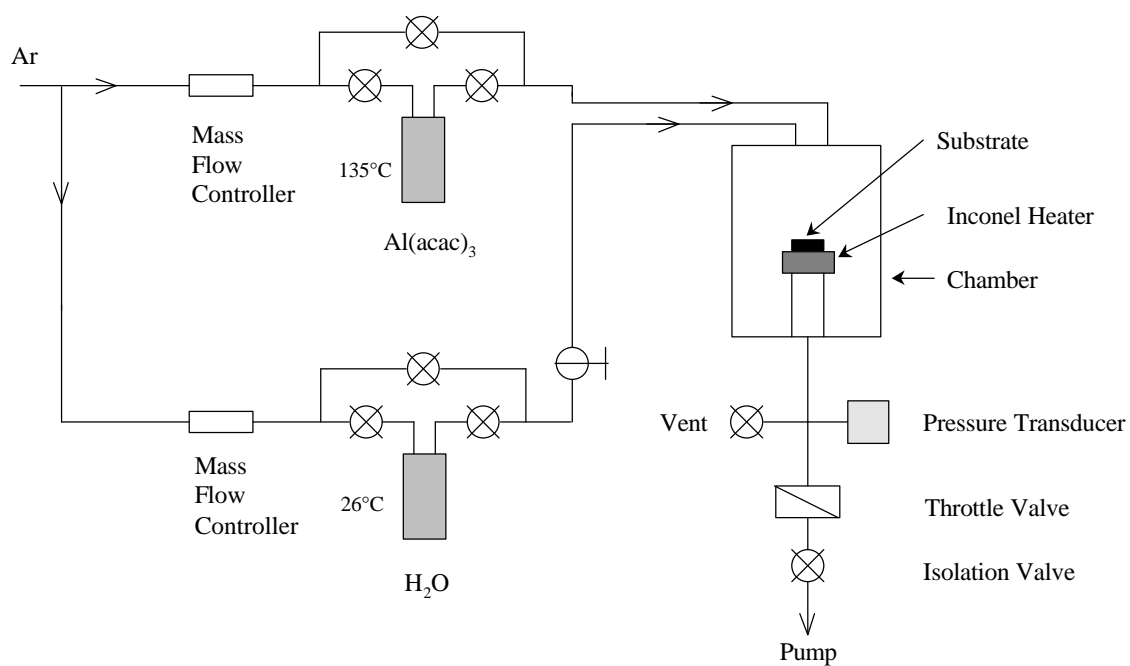
Figure 1. Schematic diagram of the MOCVD system used to deposit amorphous Al_2O_3 on various substrates.

with an upper limit of ~550°C. The system was equipped with two external vaporizers to store Al(acac)$_3$ (Sigma, CAS #13963-57-0, 99% by titration) and distilled water (produced on site). The Al(acac)$_3$ was sublimed at ~135°C (vapor pressure = 0.0047kPa) and the water was vaporized at 26°C (vapor pressure = 3.2kPa). Using mass flow controllers (MKS models #2259B and C) operating at a supply pressure of 12psi, both vapors were carried by Ar (Matheson, 99.999%) and directed to the reactor. To minimize condensation of the Al(acac)$_3$ vapor, the gas line from the vaporizer to the reactor was trace heated gradually from ~140°C to ~160°C using heating tapes. The water vapor supply line was choked with a needle valve to maintain near-atmospheric pressure in the water vaporizer.

As may be observed in the system diagram, the entrained vapors were impinged directly on the heated substrates from the gas inlets about 6 inches distant. Earlier work discussing reactor geometry demonstrated that the use of a 5" quartz "guide tube" for the precursor gasses had little effect on YSZ film morphology and thickness [C. DuBourdieu, not published]. The heater consisted of a 3 inch diameter Inconel 600 disc heated by a resistive element rod coiled to form a flat Archimedean spiral against the back face of the disc. The resistive element coil itself was rated to 950°C, but gaps between the coil and plate resulted in significant (up to 400°C) temperature gradients, despite insulation below and on the sides of the heater. Two K-type thermocouples were used to measure and control the substrate and heater temperatures. The substrate temperature was measured by placing a piece of silicon on the heater and clamping it in place with a thermocouple. This method of measurement is susceptible to error equal to the non-uniformity of the

heater surface temperature, estimated by earlier work at about ±10°C. The error, however, increases for thicker substrates such as the nickel super alloy and the APS CSZ on iron. The second thermocouple was placed between two coils of the heating element, providing direct control of the heater temperature through a Eurotherm brand temperature controller and power module.

Pressure within the reactor was controlled with a throttle valve (MKS model #253A) coupled to an exhaust valve controller (MKS model #252) and a pressure transducer (MKS Baratron model #222BA). The pressure transducer was compared to a thermocouple vacuum gauge to ensure accurate pressure readings. The pump used (Welch Duo-Seal model #1376) had an ultimate pressure of 16 Pa (120 mTorr). The over-all system ultimate pressure ranged from 53 to 67 Pa (400 to 500 mTorr), with a leak-up rate of several Torr per minute due to the fact that suspected leaks could not always be localized and eliminated.

System Operation

The operational logistics for each run of the system were as follows. First the throttle and isolation valves were closed and the system vented. Once at atmospheric pressure, the samples were loaded through an optical port level with the surface of the substrate heater. Once the samples were positioned, the port was closed and the Ar carrier gas flows turned on through the respective bypass lines. Next, the system was pumped down by opening the isolation valve and then opening the throttle valve to 15%, until the system pressure fell below 13.3kPa (100 Torr), at which time the valve was

switched to automatic control, which maintained a system pressure of 1.33kPa (10 Torr). A complete list of operating parameters may be found in Table III.

Once the system settled to the desired operational pressure, the substrate was heated to ~500°C over a period of 1-2 hours, depending on the convection load. After remaining stable for at least 15 minutes, the water vaporizer outlet was opened, the inlet opened, and the bypass valve closed. The same procedure was then performed for the $Al(acac)_3$ vaporizer. The measured run time was started at the opening of the $Al(acac)_3$ outlet valve: a necessity for runs less than 5 minutes in duration, where the initial "wave" of vapor jump-started coating growth.

Upon completion of the deposition run, the valves were put through the reverse procedure, with a 5 minute pause to allow pure Ar to flow through the two bypass lines and purge the system of precursor vapors. After the purge, the Ar supply and the substrate heater were turned off. When the substrate had cooled to below 300°C, the isolation valve was closed and the system slowly vented and allowed to cool to room temperature at atmospheric conditions until sample removal.

Thermal Annealing

All thermal annealing experiments were conducted in a small, custom-built stagnant atmosphere furnace. CSZ-coated cast iron flexure bars and free-standing CSZ coupons were all coated to a thickness of 2.5 ±0.25μm. The Si, SiC, and Ni super alloy samples were coated to thicknesses ranging from 2.55 to 0.50μm. Further investigation on Si involved coatings ranging from 0.30 to 0.040μm. The coated specimens (including

Table III. Optimized system parameters for deposition of amorphous Al_2O_3.

SYSTEM PARAMETER	*VALUE*
Substrate temperature	505-510ºC
Total system pressure	1.33 kPa
$Al(acac)_3$ bubbler temperature	135-140ºC
$Al(acac)_3$ Ar carrier gas flow rate	120 sccm*
Effective $Al(acac)_3$ flow rate	0.43-0.52 sccm
H_2O bubbler temperature	26ºC
H_2O Ar carrier gas flow rate	20 sccm
Effective H_2O flow rate	0.66 sccm

*1 sccm = 1 cm^3 / min at standard conditions.

Si substrates used for ease of characterization) were annealed in air for 20 hours over a range of 700 to 1200°C.

Sample Characterization

The as-prepared and annealed coating specimens were characterized by scanning X-ray diffraction (XRD), electron microscopy (SEM), and energy dispersive X-ray spectroscopy (EDS). The 3-step XRD process was performed first, using a diffractometer (SIEMENS model 5000, with a modified goniometer) equipped with a Cu K_a radiation source (1.4506Å, at 40kV & 30mA). First, a cursory $\theta/2\theta$ scan was performed to find a sharp, intense peak. Setting the coupled detector at the peak angle, a Phi scan was done to maximize the signal and mitigate the effects of the sample not being mounted perfectly perpendicular to the source-detector scan plane. Lastly, the sample was locked at the peak Phi value from the preceding step and an extended $\theta/2\theta$ scan conducted from 10° to 90°, stepping 0.02°/second.

Characterization with the SEM (LEO 982, field emission source) was conducted subsequent to XRD because of the necessity of carbon coating to combat sample charging. Since all coating samples are fundamentally insulators, sample charging in the SEM was quite problematic. Carbon coating (Denton Vacuum DV-502, at ~35A) of samples was used—in conjunction with carbon tape and silver paste—to mitigate the charging effects while not interfering with EDS analysis (as a gold-palladium coating would). In an effort to maintain carbon coating consistency, all samples were placed on

glass slides and carbon coated until the slides exhibited a 10-15% visual drop in transparency.

EDS was used to confirm the presence of Al_2O_3 (by its constituent elements) and assist in observing both coating presence and integrity. A typical EDS map is shown in Figure 3, an element map of the sample shown in Figure 2c. The typical EDS map– essentially a series closely spaced line scans indicating elemental intensity– is composed of 10 to 30 area scans, depending on the level of definition desired. Some of the energy windows do overlap, resulting in data redundancy, especially in complex substrates such as the René N5.

Qualitative Seal Testing – "Water Drop" Test

A simple "water drop" test was utilized to evaluate roughly the relative sealing capabilities of the Al_2O_3 coating on the highly porous CSZ substrates. This test consisted of allowing a drop of water fall from a standard 1 mm opening Pasteur pipette (Fisher Scientific 13-678-20A) on to the sample 1 cm below. Absorption of the droplet was measured for non-coated, as-coated, and annealed samples—permitting a rough comparison.

RESULTS

*Initial Coating and Annealing on Silicon*

Initial coating work was done on single crystal silicon wafers cut to ~1cm square. The as-deposited coating on Si, shown in Figure 2a, was smooth and conformal, although also amorphous. Annealing of the coated Si substrates at temperatures ranging from 700 to 1200°C resulted in extensive spallation, as shown in Figure 3. The coated specimens annealed at 700°C and 800°C (Figure 2b) exhibited somewhat less severe spallation than those annealed at the higher temperatures (Figure 2c). Samples annealed at 1100°C and 1200°C also exhibited secondary micro-cracking on non-spalled Al_2O_3, notable in Figure 2d.

To confirm the spallation observed in Figure 2, EDS was performed on the annealed sample. As may be observed in Figure 3a, there is a strong correlation of Al with the light areas seen in Figure 3c and of Si with the darker expanses. The O map (Figure 3c) appears featureless, which is likely due to significant SiO_2 formation during annealing, about 1μm was expected.

The rather extensive coating spallation significantly reduced the signal-to-noise ratio of XRD θ/2θ scans. XRD analysis was further complicated by the appearance of several unexpected metastable Al_2O_3 phases (such as θ, β, κ, and δ) [4] with their peaks in high proximity to each other—sometimes even directly overlapping other peaks of interest. The formation of silicates and other compounds on other substrates further
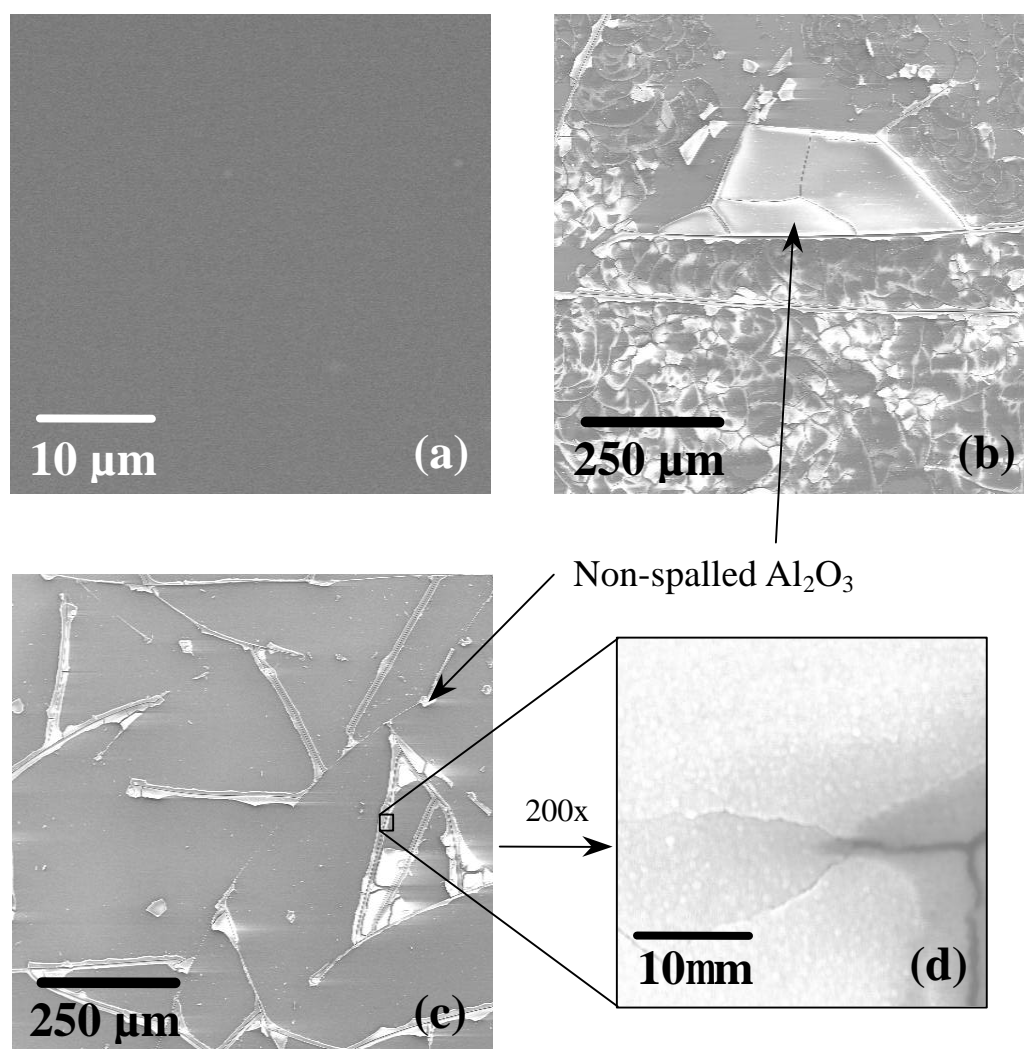
Figure 2. Al_2O_3 deposited on Si: (a) as prepared, (b) annealed at 800°C showing partial spallation, (c) annealed at 1200°C showing severe spallation, and (d) 200x (c).
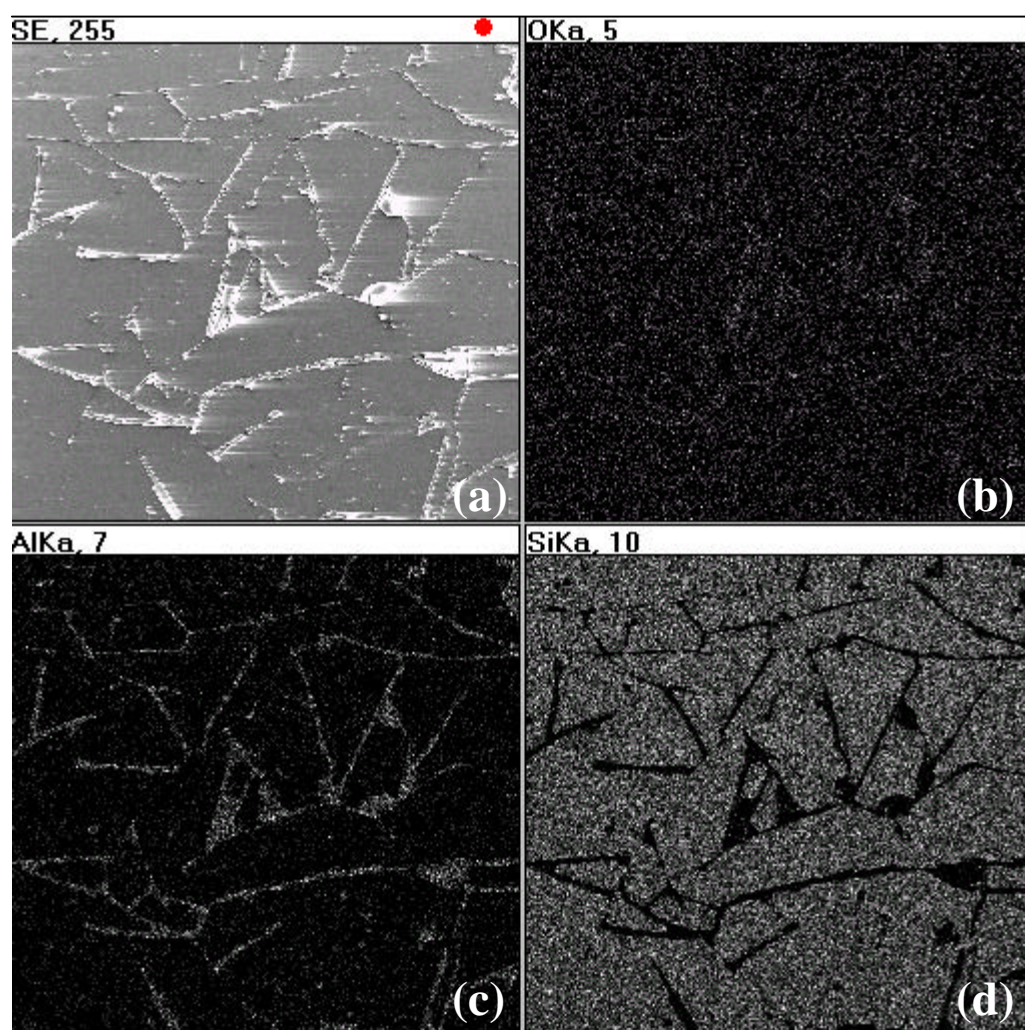
Figure 3. EDS scan of an Al_2O_3 coating deposited on silicon, which spalled after annealing at 900°C for 20 hours.
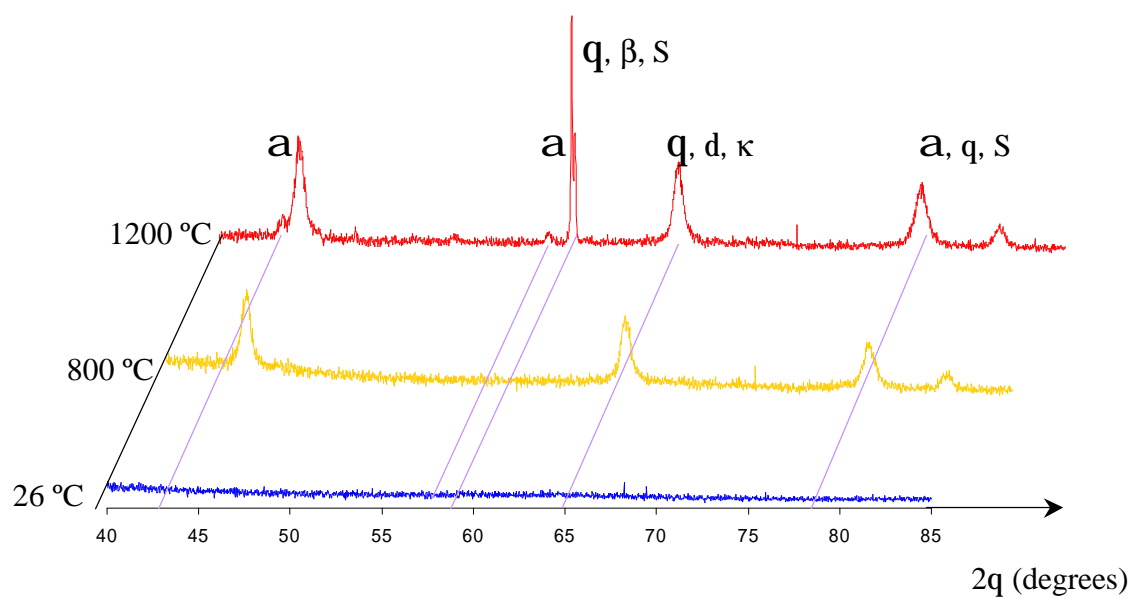
Figure 4. XRD patterns of the Al_2O_3 coating after annealing at 800°C and 1200°C (α, θ, β, κ, δ = ?-Al_2O_3, S = $Al_2Si_4O_{10}$).

hampered characterization efforts. Despite these complications, Figure 4 shows that the crystallization of the amorphous coating to metastable- and α-Al_2O_3 occurred rapidly during the increasing thermal exposures.

The limiting initial parameters of the investigation, namely process temperature, relegated deposition to amorphous Al_2O_3. The spallation resulted primarily from the significant volume shrinkage associated with transformation to the primary metastable phase – θ-Al_2O_3. The porous CSZ TBC samples are expected to be better able to absorb the crystallization-induced stresses than the silicon, SiC, and René N5.

Coating of APS CSZ Samples

Al_2O_3 coating deposited on the CSZ-coated cast iron and free-standing CSZ substrates exhibited a nodular morphology across its conforming contour, as shown in Figure 5a. Annealing of the samples, however, lead to cracking at temperatures as low as 700°C, where intermediate Al_2O_3 phases took over from the original amorphous coating. Along with advancing crystallization, coating morphology appeared to smoothen with increasing temperature, as may be observed in Figures 5b and 5c, where the nodular quality of the coating appears to recede. A general smoothing is also discernable between as-coated (Figure 5a) and any of the annealed coating samples.

Despite extensive microcracking due to volume shrinkage during crystallization, no spallation of the coating occurred (see Figures 5 and 6). In general, the degree (and width) of microcracking increased with annealing temperature (seen in Figures 6a and 6b), as crystallization was driven further towards completion and α-Al_2O_3, the most
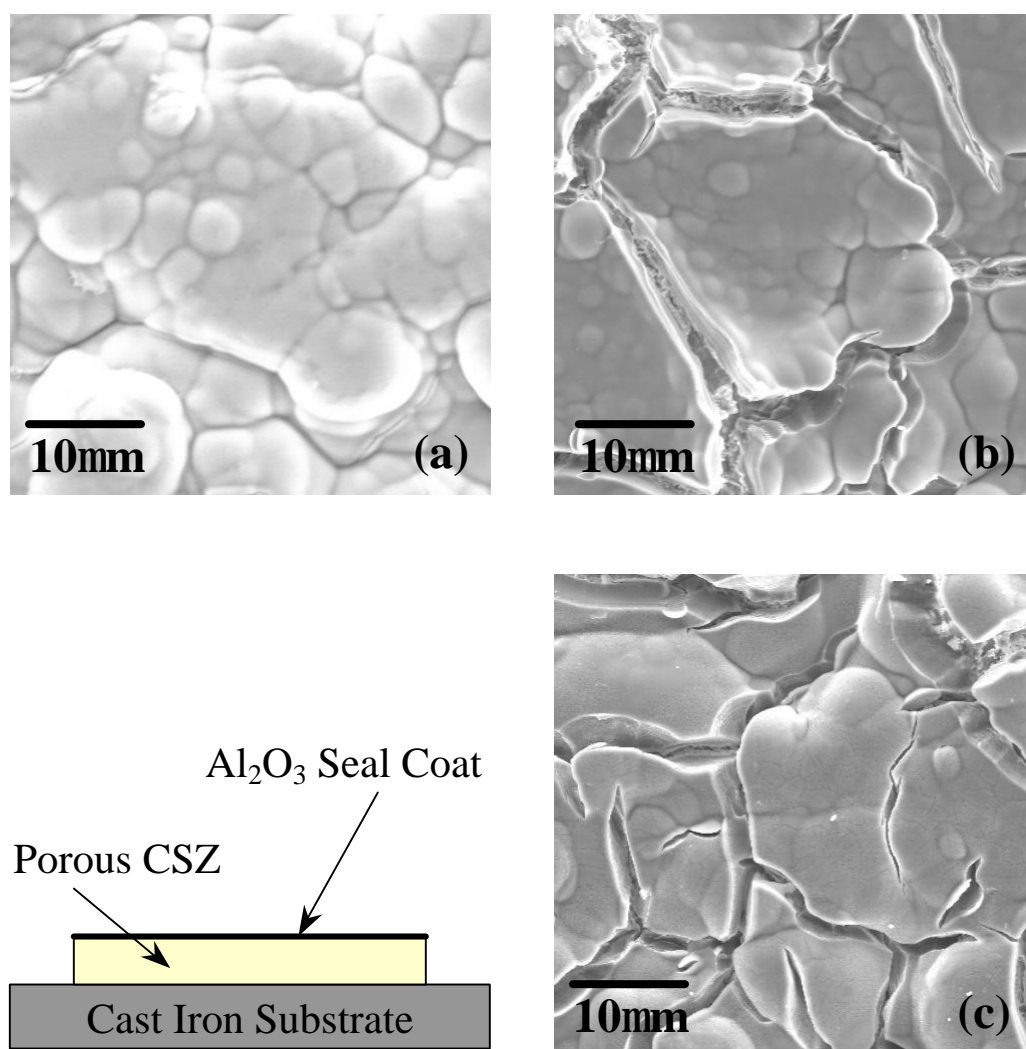
Figure 5. Al$_2$O$_3$ deposited CSZ-coated cast iron: (a) as prepared, (b) annealed at 700°C, and (c) annealed at 1000°C.

Al$_2$O$_3$ Seal Coat

Porous CSZ

No Iron Substrate
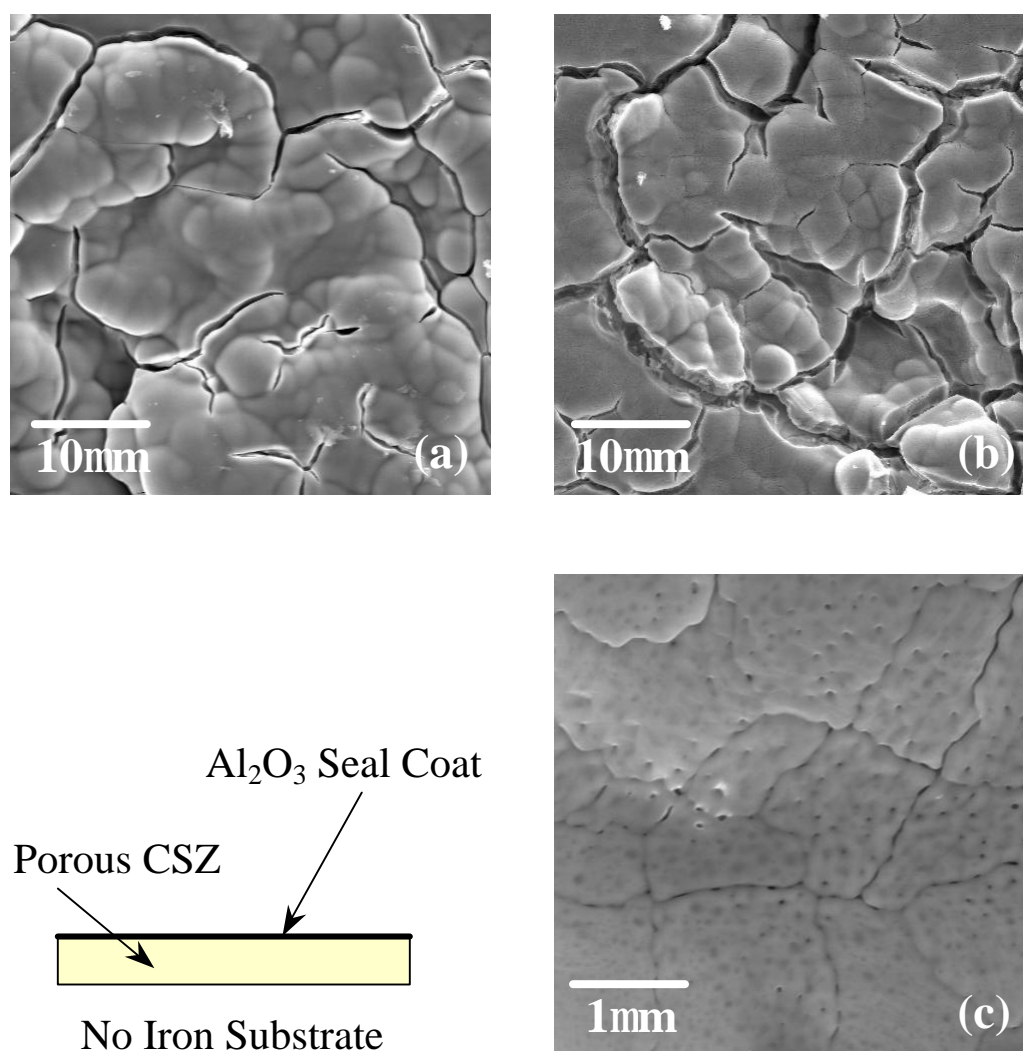
Figure 6. Al$_2$O$_3$ deposited on free-standing CSZ: (a) annealed at 700°C, (b) and (c) annealed at 1100°C.

thermodynamically stable phase. The highly porous—and thus strain-tolerant—nature of the CSZ TBC, together with the greater degree of mechanical interlocking, accounts for the superior coating adhesion observed during and after annealing.

Secondary features were evident in coating samples annealed at 1000 and 1100°C. Visible in Figure 6c are pores and what appear to be grain boundaries. The pores almost certainly agglomerated during secondary and tertiary crystallization steps, where the volume shrinkage is significantly smaller than the amorphous to θ-Al_2O_3 transformation of –9%. This manifestation of stress relief, due to the size of the pores, could not account for the lack of sealing seen in the qualitative "water drop" test— whereas the considerably larger mud-cracking pattern in the Al_2O_3 coating could account for it.

The rudimentary water drop test showed a greatly heightened residence time on the coated samples. Droplets on non-coated samples were wetting and were absorbed in about 4 minutes. Droplets on coated, non-annealed samples were slightly wetting and evaporated in ~ 40 minutes; while droplets on coated, annealed samples were absorbed in under 5 minutes. Reference drops were placed on a glass slide (highly wetting) and a cast iron bar (non-wetting): evaporation times were 60 and 85 minutes, respectively.

Coating of Silicon Carbide Samples

Al_2O_3 coating deposited on polished SiC appeared conformal, but exhibited a considerable number of 1-5μm diameter pits, covering about 1% of the substrate surface

27
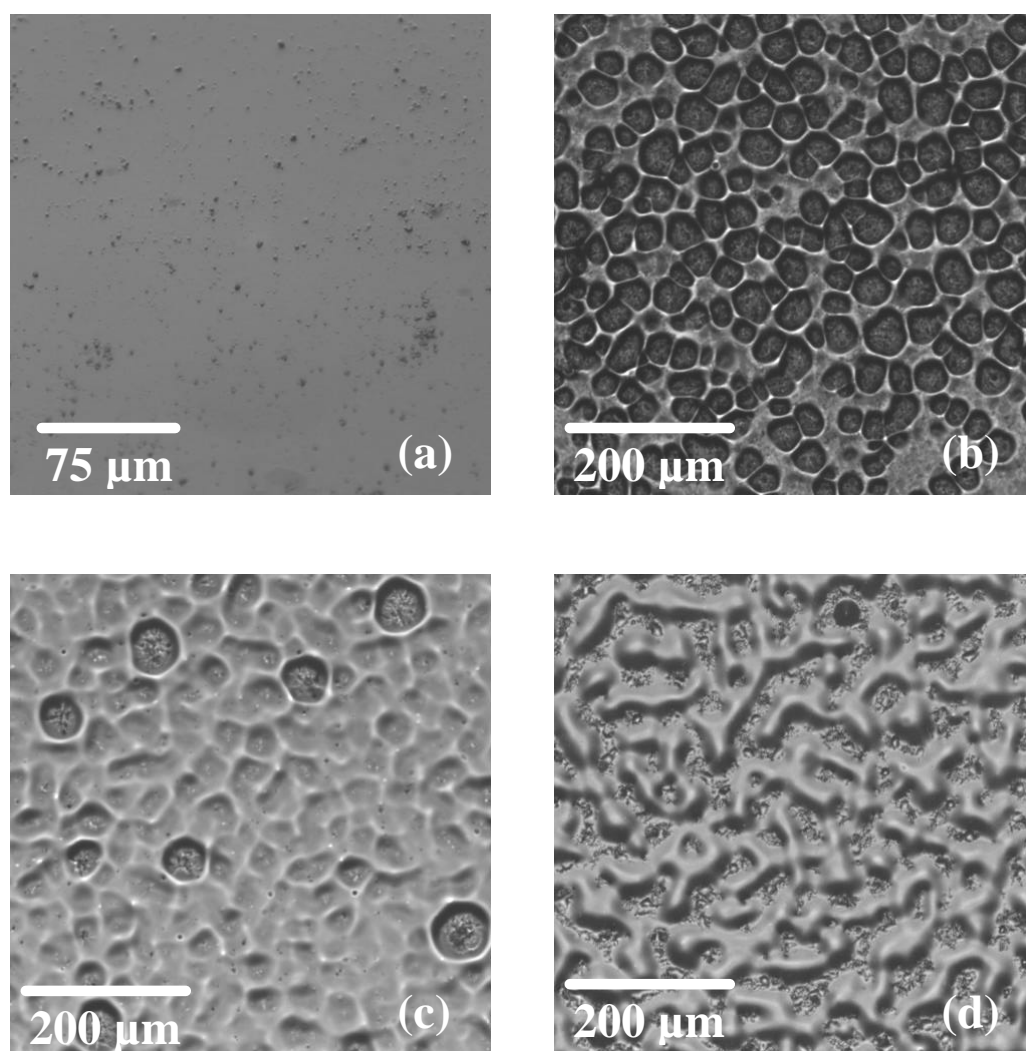
Figure 7. Amorphous Al$_2$O$_3$ coating deposited on SiC to a thickness of: (a) 770nm as deposited, (b) 880nm and annealed, (c) 830nm and annealed, and (d) 510nm and annealed.

area. Upon annealing, however, these defects appear to be eclipsed by crater formation in the two ~800nm coating samples in Figures 7b & 7c. Annealing of the thinnest sample, shown in Figure 7d, resulted in a "pooling" effect in an apparent effort to minimize either surface area, substrate/coating interface energy, or both. The annealed coatings on SiC exhibited no spallation, most likely due to the relief of stresses during coating diffusion.

Coating of Nickel Super Alloy (René N5)

The amorphous Al_2O_3 deposited on the René N5 nickel super alloy exhibited striations in addition to the significant pore systems observed in Figure 8a. Upon annealing of the ~1mm coating in Figure 8c, there appears to be a slight filling in of the pores. In an annealed coating half as thick, shown in Figure 8d, the pore presence is further reduced, though barely to 50% of as deposited, and a cross-hatch pattern begins to emerge. As the substrate is a single crystal and essentially featureless (certainly devoid of polishing artifacts), it is not certain where this cross-hatching originates, unless it is instigated by the FCC structure of the substrate.

Summary of Substrate Effects

The Al_2O_3 coating on Si exhibited considerable spallation due to both CTE mismatch strains (~+0.5%) and the volume shrinkage associated with crystallization of the amorphous coating (> -9%). In contrast, the Al_2O_3 coating on the CSZ surface,
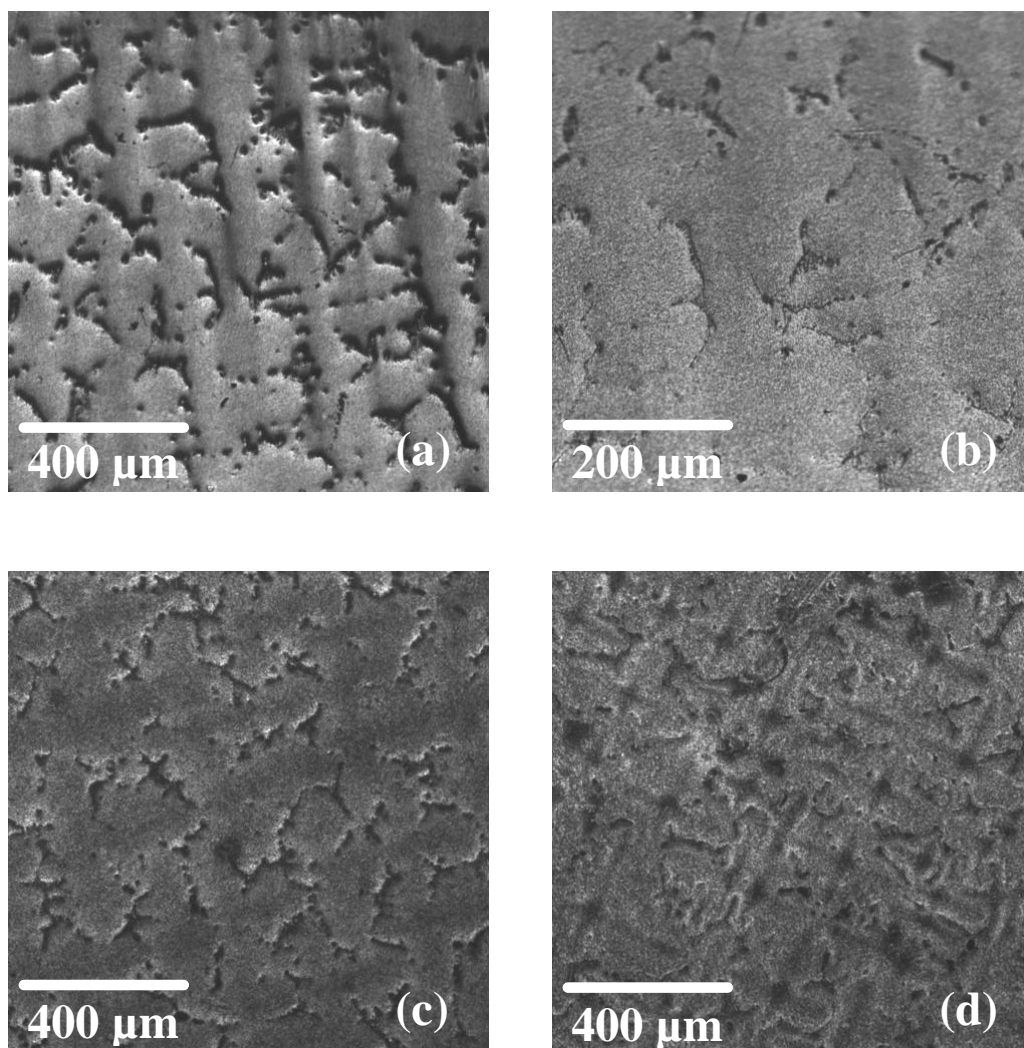
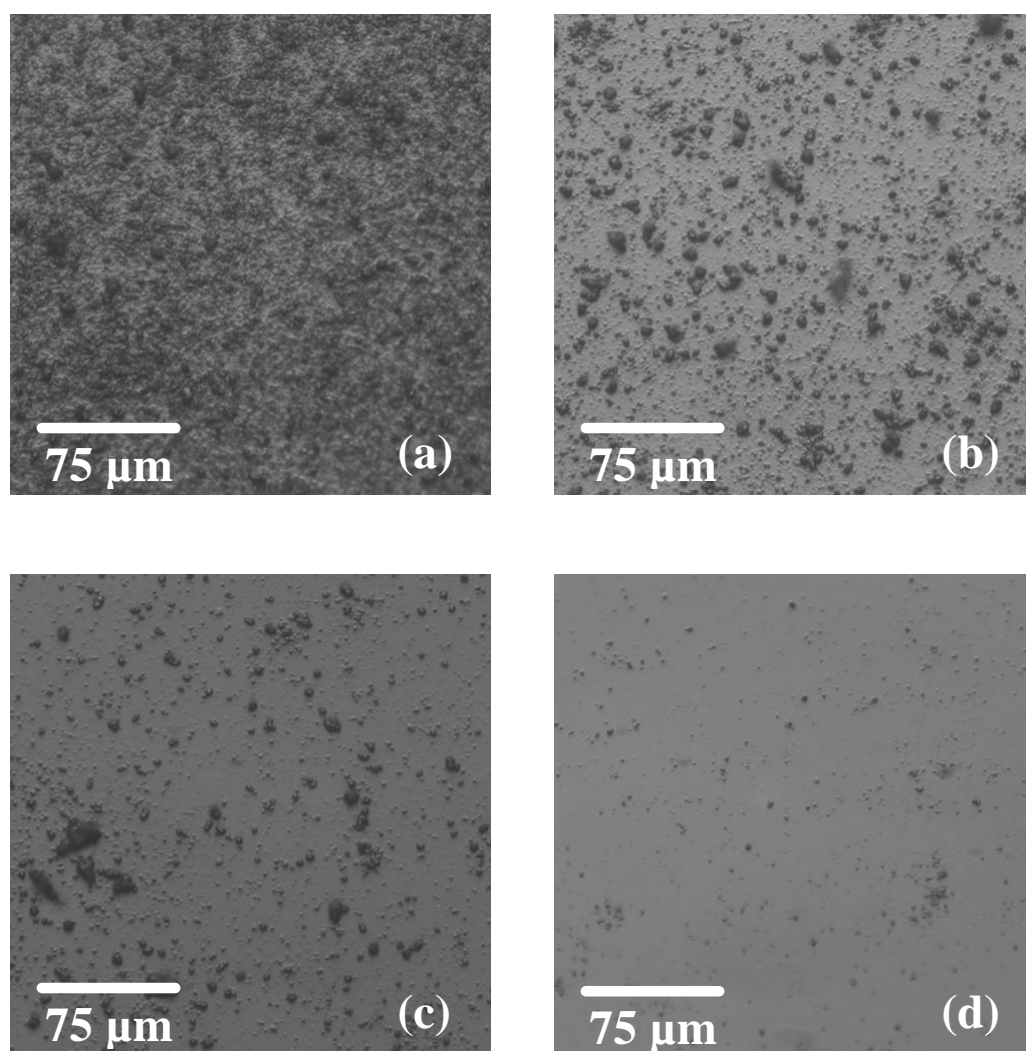**Figure 8**. Amorphous Al_2O_3 coating deposited on René N5: (a) as deposited to 760nm (b) at 2x (a), (c) to 960nm and annealed, and (d) to 540nm and annealed,-- with a surface cross-hatch pattern emerging.

whether free-standing or on cast iron, did adhere well to the substrate, although it microcracked extensively. The adhesion of the coating on the CSZ surface was attributed to: (1) mechanical interlocking at the Al_2O_3-CSZ interface and, (2) lower residual stresses at the interface due to the lower CTE mismatch between Al_2O_3 and CSZ. Nevertheless, the Al_2O_3 coating on the CSZ surface is expected to be inadequate for sealing the porous CSZ surface because of the observed microcracking of the coating upon annealing.

Similar to the Si and APS CSZ, the coatings deposited on SiC and René N5 were dense and fully conformal, though pores/pits were incorporated unexpectedly. Annealing did not result in spallation, due primarily to the strain-tolerating pores. The sub-micron coatings on each substrate generated unique morphological characteristics during annealing—especially notable at the lower end, around 500nm.

Substrate variation did appear to have an effect on the nucleation of amorphous Al_2O_3. As may be observed in Figure 9a, the coating deposited on Si exhibited heavy nucleation, creating an almost continuous, though nodular, coating. Single crystal Al_2O_3 (Figure 9b) also exhibits significant nuclei, covering about 20% of the sample's surface area after 20 minutes of deposition. The single crystal René N5 (Figure 9c) and the SiC (Figure 9d) exhibit only moderate nucleation after the same 20 minutes. As all samples were polished to a fine finish and located adjacent to each other on the substrate heater, it is not yet clear if amorphous Al_2O_3 possesses an affinity for any particular substrate group.

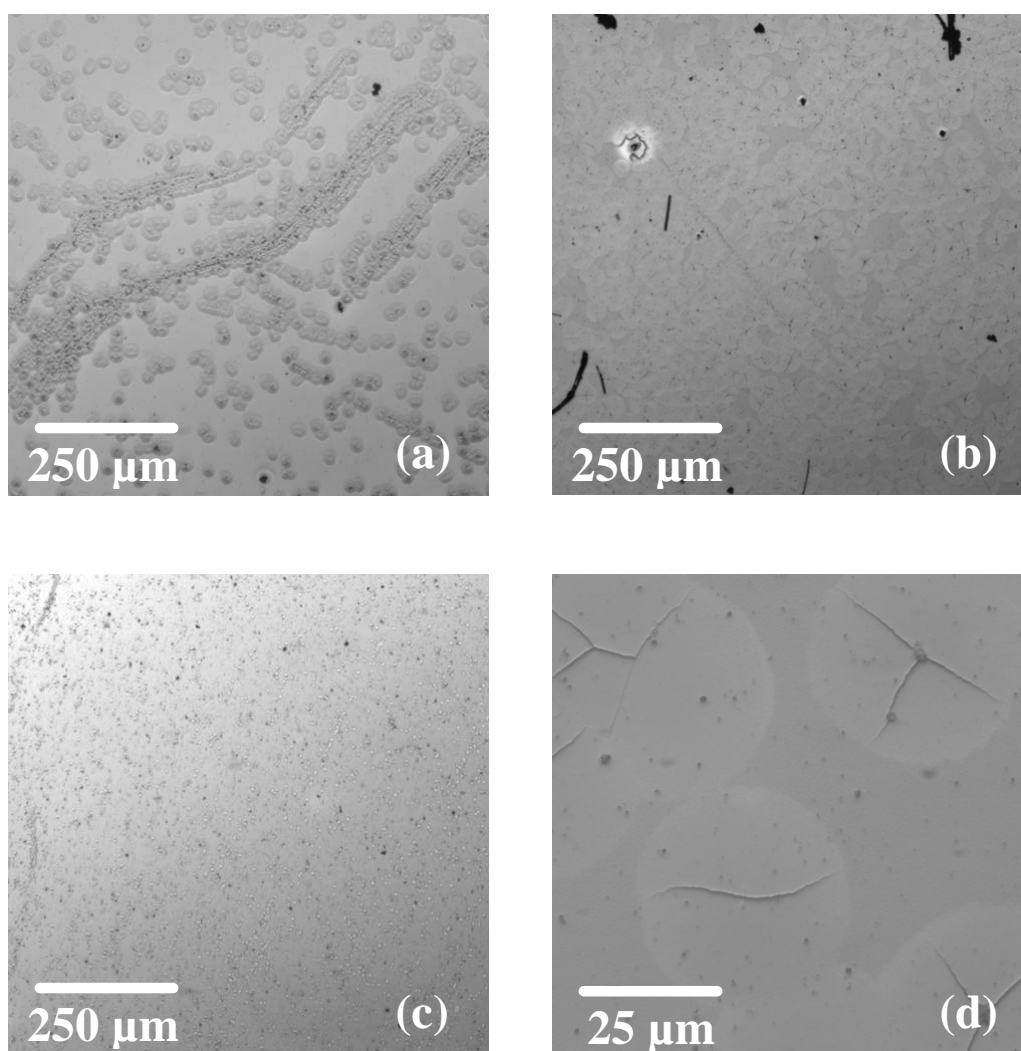**Figure 9**. Amorphous Al_2O_3 coating deposited on: (a) 100 Si, (b) single crystal Al_2O_3, (c) René N5, and (d) SiC.

Sub-micron Al₂O₃ Coating Evaluation

With the strong morphological differences observed on different substrates with sub-micron coatings, further exploration was conducted. Work by F.F. Lange [31,32] stipulates that stress relief through cracking is a function of material constants and depends directly on film thickness. Thus there exists a critical film thickness associated with a maximum internal energy, up to which a material will be able to contain tensile (or compressive) stresses generated by crystallization or mismatch of coefficients of thermal expansion. For most materials, this value resides close to 100nm for tensile stress.

Sub-micron coatings on silicon showed greatly heightened adhesion during annealing. Figure 10 shows coatings of decreasing thickness from 290nm (10a) to 160 (10c), all of which were annealed at 1100°C for 20 hours. Crack initiation in these films results from the coalescing of many of the "pockets" of plastic deformation readily observable in Figure 10d. The thickest coating exhibits the most notable alignment of these pockets, which are in the process of initiating a crack in the coating in Figure 10a. In Figure 10b, the pockets have not yet begun to align and manifest themselves in the two smatterings of low-contrast tones of the figure. The pockets are completely absent from the thinnest coating (160nm), only the apparent pores, observed previously on silicon, remain.

The two thinnest coating samples, 70nm and 40nm, are shown after annealing in Figure 11. The wavy texture induced in the film by annealing may be an attempt at minor stress relaxation, similar to that observed on the SiC in Figure 7d; the nearest anomaly comparable to a crack of any significance may be found in Figure 11d, which

Figure 10. Sub-micron Al$_2$O$_3$ coating deposited on silicon and annealed at 1100°C: (a) 290nm, (b) 260nm, (c) 160nm, and (d) 160nm.
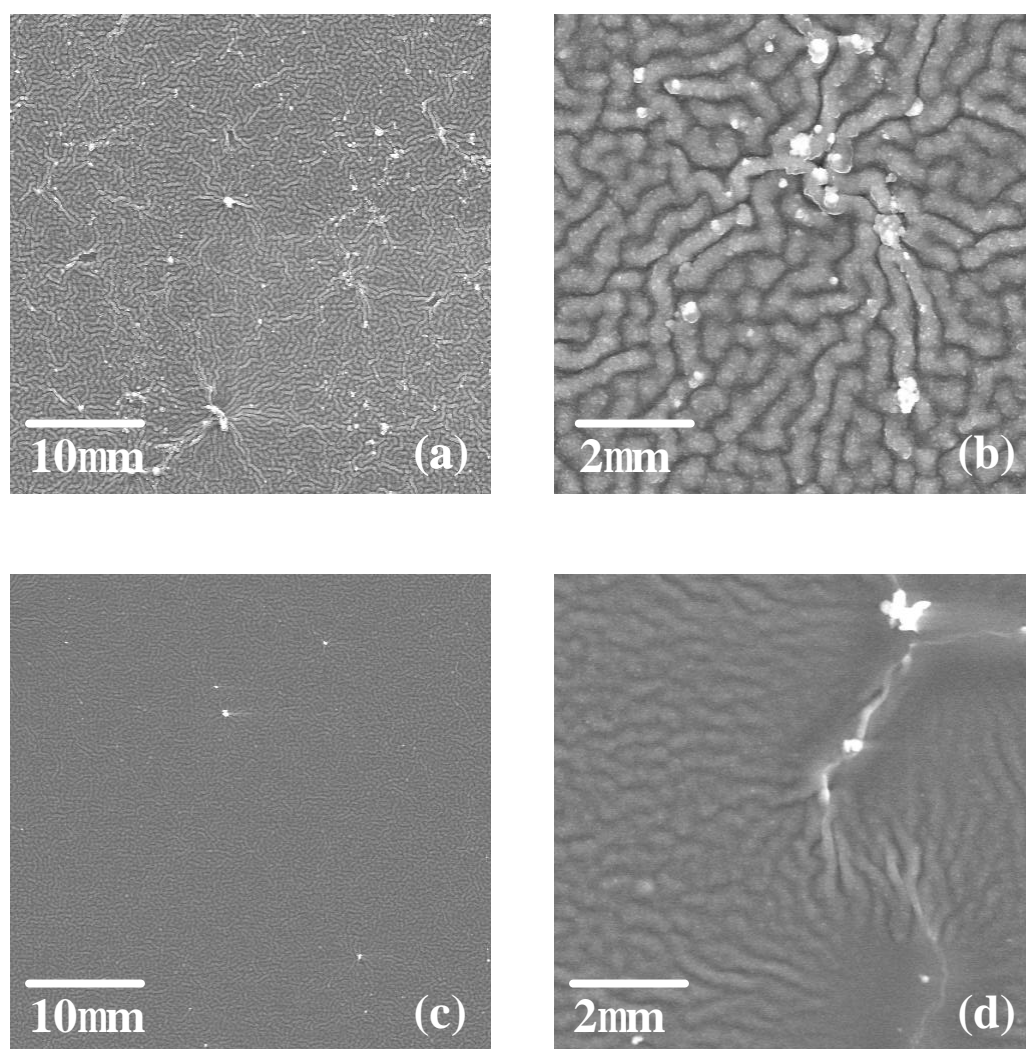
Figure 11. Al$_2$O$_3$ deposited on Si and annealed: (a) and (b) 70nm, (c) and (d) 40nm.

resembles slightly one of the pockets of deformation found in Figure 10d. It is also of interest that the texture of the thinner coating is proportionally finer than that of the thicker coating.

While annealing of thick (2.25μm) MOCVD Al_2O_3 coatings leads to extensive microcracking, thin coatings survive annealing because the reduced strain energy no longer forces crack propagation to reduce the over-all free energy of the film. Figure 12 demonstrates the crystalline nature of the sub-100nm coatings depicted in Figures 10b & 10d. A small area on each was observed to have spalled where several super-fine cracks come together. These "sub-features," it must be noted, are not representative; being few and far between.
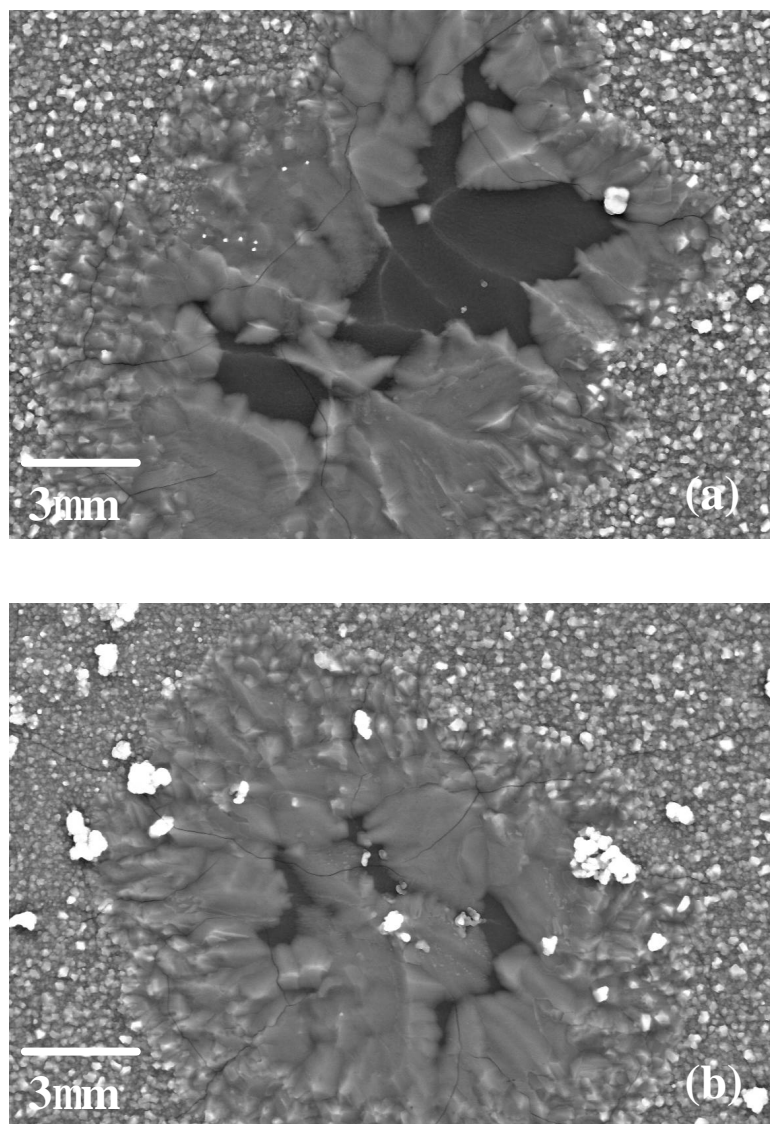
Figure 12. Al$_2$O$_3$ deposited on Si and annealed: (a) 70nm, and (b) 70nm—showing small areas of spallation in the crystallized coating.

Discussion

Nucleation and Growth of Vapor-Deposited Al$_2$O$_3$

Nucleation of alumina films depends on well understood factors. The two most prevalent factors in any CVD system are precursor partial pressure and deposition temperature. The nucleus density is highly correlated to the supersaturation of the deposited material and, thus, also to the precursor concentrations in the reaction atmosphere. The temperature of the substrate is of considerable importance, too. An increase in temperature generally results in a decrease in nucleus density, as surface migration (hence, coalescence of nuclei) and desorption are more heavily favored. The combination of these two factors allows for possible morphological control of films: high growth rates result in less ordered and crystalline films (or sometimes whiskers or other phenomena observed in later work) and low growth rates generally produce more highly ordered, better adhering films [5] with noticeable grain refinement [24]. As all coatings deposited were amorphous, control of the structure through reduced growth rate is not probable. If a metastable phase such as θ-Al$_2$O$_3$ were deposited (as desired), growth rate control would take on a more important roll in the crystallization and transformation to α-Al$_2$O$_3$.

Effect of Substrate and Pressure

Another consideration for nucleation is the effect of the initial substrate surface. Variations in the substrate will adversely affect nucleus density – which will, in turn,

affect film adhesion [25]. The non-uniform phase distribution found in cemented carbide tool tips, for example, results in a varied nucleus density and later, grain size. Variations have been demonstrated across many substrates, with no discernable pattern of morphological or substrate orientation dependencies [25-27]. The coatings produced during the course of this work did not permit any significant elucidation.

Both the Si and the APS CSZ substrates effected an morphological influence on the amorphous Al_2O_3 deposited. In the case of Si the coating was nearly as smooth as the originally polished substrate. The random/complex APS CSZ (constraint by the iron bar had no effect) substrates resulted in a highly nodular coating, where the periphery of each CSZ platelet is the source of multiple low energy—nucleation—sites. As noted in the results, the coating deposited on SiC was relatively smooth, but with pits in evidence. Similarly, the René N5 coating was pitted, though more severely so, and the coating also appeared striated.

In addition to precursor partial pressures, which are very sensitive to their respective vaporization temperatures, overall system pressure is of some importance. Generally, low system pressures are favored for precursor decomposition common with MOCVD reactions, where gaseous products out-weigh the reactants. However, this favoritism is balanced by the necessity of maintaining a material source. Reports have confirmed this, indicating a roughly linear increase in growth rate with a total pressure of up to ~6.7kPa (50 Torr) [21]. Some experiments were carried out at higher system pressures (up to 101.3kPa), but system deficiencies and problems eroded any confidence to be had in these samples.
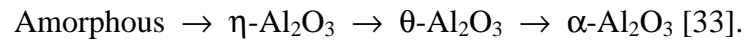
Transformation During Growth

Sustained growth is another consideration for coating deposition. Temperature determines morphology and phase deposition as well as transformation kinetics. Together with processing time, temperature has a profound effect on morphology. As discussed above, precursor partial pressures may be used to control deposition and growth rate by depriving the reacting system of a sufficient amount of a vital constituent—in essence "choking" the process and effecting control on the reaction rate. This will also affect the morphology.

Once the coating has been deposited, transformation to α-Al_2O_3 is inevitable with the investment of/subjection to any significant amount of thermal energy. Transformation to the next phase, whether it be another metastable phase or α-Al_2O_3, occurs most often at any combination of three places: the substrate surface, grain boundary nodes, and coating crack edges. The coating/substrate interface is a favored nucleation point in crystallization of coated specimens. As the coating transforms, a "rising front" is created as the phase boundary migrates up towards the coating surface. Grain boundary nodes are another favored nucleation point, as are crack edges. These have a tendency to lead to the intermediary, two-layer system until crystallization is complete [25]. This progression can lead to complex stress systems as uneven volume shrinkage reduces coating adhesion.

The phase transformation of an annealed coating depends primarily on the starting material (precursor) and the temperature at which it is deposited (and what phase it forms) [28,29]. There are several well-defined paths based on various deposited

metastable polymorphs from common precursors [4]. Factors which further affect the phase transition path during crystallization include annealing parameters, impurities, crystallinity, and atmosphere exposure. The coatings evaluated to create Figure 4 appear to follow the Bayerite source path:

$$\text{Amorphous} \rightarrow \eta\text{-Al}_2\text{O}_3 \rightarrow \theta\text{-Al}_2\text{O}_3 \rightarrow \alpha\text{-Al}_2\text{O}_3 \text{ [33]}.$$

The coatings appear to skip the eta phase, during annealing, and progress directly to a θ / β mixture before transforming to α-Al$_2$O$_3$. Despite the morphological peculiarities of the thin films, which appeared to follow the same transformation path, the fine microstructure, a cauliflower-like nodule-upon-nodule structure, has been observed before with the deposition of α-Al$_2$O$_3$ phase [4]. The cracking and transformation observed in the finer features also match well with the understood nucleation mechanisms associated with the final transformation. All spallation occurs at the super-fine crack vertices observed in Figure 12, which is consistent with the preferential nucleation transformation site of α-Al$_2$O$_3$.

CONCLUSIONS

The metal-organic precursor Al(acac)$_3$, coupled with water, is a safe and convenient low-temperature precursor for CVD of Al$_2$O$_3$. However, it suffers the same disadvantages as other precursor systems—deposition of only amorphous-Al$_2$O$_3$ below 500°C. Using this precursor system, a uniform amorphous-Al$_2$O$_3$ coating was prepared on a porous CSZ substrate, SiC, and nickel super alloy René N5 at ~500°C. Annealing of the sub-micron coatings on SiC revealed an inherent morphological instability. The nickel-based substrates did not suffer from instability, but did demonstrate defects in the as-deposited coating—which survived annealing.

Thermal annealing of the thick Al$_2$O$_3$-coated CSZ substrates resulted in significant microcracking of the coating, mainly because of the volume shrinkage induced by the crystallization of the amorphous coating to metastable- and α-Al$_2$O$_3$ phases. The crystallization occurred at temperatures as low as 700°C within 20 hours; only sub-micron coatings remained intact subsequent to annealing. These observations indicate that a thick amorphous Al$_2$O$_3$ coating, although it can be prepared at ~500°C as a conformal and uniform coating, would not be useful as a seal coating for the CSZ TBC coating application. This study demonstrates Al$_2$O$_3$ must be deposited as a crystalline coating (preferably in the thermodynamically stable α-Al$_2$O$_3$ phase, minimally in the metastable θ-Al$_2$O$_3$ phase) to mitigate the adverse effects of volume shrinkage caused by crystallization.

FUTURE WORK

Sub-micron coatings would very likely have difficulty sealing the complex surface of a TBC such as that of the APS CSZ seen here. Their ability to contain stress indicates a potential to overcome the volume shrinkage during crystallization problem— leaving the door open for investigation of thicker coatings formed by multiple alternating deposition and annealing steps.

Coatings on SiC did not appear to be morphologically stable, and thus may require higher thickness to overcome interface/surface energy inclinations. René N5, on the other hand, appears to be stable, and slower coating growth rates may eradicate coating defects, although these defects may be absorbing the transformation stresses.

REFERENCES

1. J.T. DeMasi-Marcin and D.K. Gupta, "Protective Coatings in the Gas Turbine Engine," *Surf.Coat. Tech.*, **68/69** 1 (1994).

2. M. Brad Beardsley, "Application of Thick Thermal Barrier Coatings to Diesel Engines," *Proceedings of the 1990 Coatings for Advanced Heat Engines Workshop,* pp. II-53 – II-56.

3. T.M. Yonushonis, H.K. HG, and R.C. Novak, "Thick Thermal Barrier Coatings for Diesel Engines," *Proceedings of the 1990 Coatings for Advanced Heat Engines Workshop,* pp. II-45 – II-51.

4. E. Fredriksson and J.-O. Carlsson, "Chemical Vapour Deposition of Aluminum Oxides from Various Gas Mixtures," *J. of Chemical Vapor Deposition,* **1** (4) 333-417 (1993).

5. B. Lux, C. Colombier, H. Altena, and K. Stjernberg, "Preparation of Alumina Coatings by Chemical Vapor Deposition," *Thin Solid Films,* **138** 49-64 (1986).

6. K. Iida and T. Tsujide, "Physical and Chemical Properties of Aluminum Oxide Films Deposited by $AlCl_3$-CO_2-H_2 System," *Jpn. J. Appl. Phys.*, **11** (6): 840-849 (1972).

7. S.K. Tung and R.E. Caffrey, "Pyrolytic Deposition and Properties of Aluminum Oxide Films," *J. Electrochem. Soc.*, **114** 275C (1967).

8. R. Funk, H. Schachner, C. Triquet, M. Kornmann and B. Lux, "Coating of Cemented Carbide Cutting Tools with Alumina by Chemical Vapour Deposition," *J. Electrochem. Soc.*, **123** (2) 285-289 (1976).

9. R. Colmet and R. Naslain, "Chemical Vapour Deposition of Alumina on Cutting Tool Inserts from $AlCl_3$-H_2-CO_2 Mixtures: Influence of the Chemical Vapour Deposition Parameters and the Nature of the Inserts on the Morphology and Wear Resistance of the Coatings," *Wear*, **80** 221-231 (1982).

10. J. Lindstrom and H. Schachner, "Non-Equilibrium Conditions for CVD of Alumina," *Proc. 3rd Eur. Conf. CVD*, H.E. Hintermann, editor, LSRH, Neuchatel, Switzerland, pp. 208-217 (1980).

11. S.W. Choi, C. Kim, J.G. Kim and J.S. Chun, "Nucleation and Growth of Aluminium Oxide on Silicon in the CVD Process," *J. Mater. Sci.*, **22** 1051-1056 (1987).

12. P.S. Schaffer, "Vapor-Phase Growth of Alpha Alumina Single Crystals," *J. Am. Ceram. Soc.*, **46** (10) 508-511 (1965).

13. Sampuran-Sing and K.V. Anand, "Electrochemical Properties of Dielectric Films of Aluminium Oxide Deposited on Silicon," *Thin Solid Films*, **37** 453-460 (1976).

14. G.L. Tingey, "Kinetics of the Water-Gas Equilibrium Reaction I: The Reaction of Carbon Dioxide with Hydrogen," *J. of Phys. Chem.* **70** (5) 1406-1412 (1966).

15. J. Saraie, J. Kwon and Y. Yodogawa, "Chemical Vapour Deposition of Al2O3 Thin Films under Reduced Pressures," *J. Electrochem. Soc.*, **132** (4) 890-892 (1985).

16. M.T. Duffy and W. Kern, "Chemical Vapor Deposition of Aluminum Oxide Films from Organo-Aluminum Compounds," *RCA Rev.*, 754-771 (1970).

17. M. Ishida, I. Katakabe, T. Nakamura and N. Ohtake, "Epitaxial Al2O3 Films on Si by Low-Pressure Chemical Vapor Deposition," *Appl. Phys. Lett.*, **52** (16) 1326-1328 (1988).

18. L.H. Hall and W.C. Robinette, "Properties of Aluminum Oxide Films Obtained from Nitrous Oxide an Aluminum Trimethyl," *J. Electrochem. Soc.*, **118** (10) 1624-1626 (1971).

19. M.L. Lazarov, M.I. Martchovska and G. Yanakiev, "Films of Aluminum Oxide from Microelectronic Purposes," *Bulg. J. Phys.*, **II** (6) 622-627 (1975).

20. M. Matsushita and Y. Koga, "Thin Alumina Films Prepared by Thermal Decomposition of Aluminum Triethoxide," *133rd Nat. Meet. Electrochem. Soc.*, Abstract No. 90, pp. 230-231 (1968).

21. T. Maruyama and S. Arai, "Aluminum oxide thin films prepared by chemical vapor deposition from aluminum acetylacetonate," *Appl. Phys. Lett.,* **60** (3) 322-323 (1992).

22. J.S. Kim, H.A. Marzouk, P.J. Reucroft, J.D. Robertson, and C.E. Hamrin, Jr., "Effect of water vapor on the growth of aluminum oxide films by low pressure chemical vapor deposition," *Thin Solid Films,* 230 (1993) 156-159.

23. V.M. Koleshko, V.V. Sviridov, V.P. Boldyrev, B.S. Reznikov, I.V. Nekaryukin, K.D. Yashin, N.N. Goroshko and A.A. Kovalevskii, "Preparation of Al2O3 Films by Pyrolysis of Al Acetylacetonate," *Inorg. Mater.*, **12** 1783-1785 (1976).

24. S. Vuorinen and L. Karlsson, "Phase Transformation in Chemically Vapour-deposited κ-alumina," *Thin Solid Films,* **214** 132-143 (1992).

25. N. Lindulf, M. Halvarsson, H. Norden, and S. Vuorinen, "Microstructural Investigation of the κ-Al$_2$O$_3$? α-Al$_2$O$_3$ Transformation in Multilayer Coatings of Chemically Vapor Deposited k-Al2O3," *Thin Solid Films*, **253** 311-317 (1994).

26. T.W. Simpson, Q. Wen, N. Yu, and D.R. Clarke, "Kinetics o the Amorphous ? γ ? α Transformations in Aluminum Oxide: Effect of Crystallographic Orientation," *J. Am. Ceram. Soc.,* **81** (1) 61-66 (1998).

27. R. Colmet and R. Naslain, "Chemical Vapour Deposition of Alumina on Cutting Tool Inserts from AlCl$_3$-H$_2$-CO$_2$ Mixtures: Influence of the Chemical Vapour Deposition Parameters and the Nature of the Inserts on the Morphology and Wear Resistance of the Coatings," *Wear,* **80** 221-231 (1982).

28. E. Fredriksson and J.-O. Carlsson, "Phase Transformation During CVD of Aluminum Oxide," *Journal De Physique,* **50** (5) 391-399 (1989).

29. I. Levin and D. Brandon, "Metastable Alumina Polymorphs: Crystal Structures and Transition Sequences," *J. Am. Ceram. Soc.,* **81** (8) 1995-2012 (1998).

30. V.P. Boldyrev, V.M. Koleshko, B.S. Reznikov, I.V. Nekaryukin, L.D. Buiko, and K.D. Yashin, "Structure and Properties of Al2O3 Films Obtained by Pyrolysis of Aluminum Acetylacetonate," Translated from: *Izvestiya Akademii Nauk SSSR, Neorganicheskie Materialy,* **12** (12) 2181-2184 (1976).

31. F.F. Lange, "Chemical Solution Routes to Single-Crystal Thin Films," *Science*, **273** 903-908 (1996).

32. S. Ho, C. Hillman, F.F. Lange and Z. Suo, "Surface Cracking in Layers Under Biaxial, Residual Compressive Stress," *J. Am. Ceram. Soc.*, **78** (9) 2353-2359 (1995).

33. W. H. Gitzen, editor, "Alumina as a Ceramic Material," *Am. Ceram. Soc.*, 14-35 (1970).